CrossMark

LAMOST J040643.69+542347.8: The Fastest Rotator in the Galaxy

Guang-Wei Li (李广-伟) [ORCID]
Key laboratory of Space Astronomy and Technology, National Astronomical Observatories, Chinese Academy of Sciences, Beijing 100101, People's Republic of China; lgw@bao.ac.cn

Abstract

Rotation and binary interaction play important roles in understanding the nature of massive stars ($\gtrsim 8 M_\odot$). Some interesting transients, such as the long-duration gamma-ray bursts, are thought to be originated from fast-rotating massive stars. Because the strong stellar wind can effectively spin down a metal-rich massive star with fast rotation, it is very hard to find single massive stars rotating critically in the Galaxy. In the present work reported is the discovery of the fastest rotator in the Galaxy, LAMOST J040643.69+542347.8, with a projected rotational velocity $v_e \sin i \sim 540$ km s^{-1}, which is ~ 100 km s^{-1} faster than that of the previous record holder HD 191423. The star has a spectral type of O6.5 Vnnn(f)p. Its He I $\lambda 4471$ absorption line is blueshifted and asymmetric, while its He II $\lambda 4686$ and Hα have central absorption reversals in their emissions. It is also a runaway star, which implies an origin in a close binary interaction. Compared to VFTS 285 and VFTS 102 (their $v_e \sin i \sim 610$ km s^{-1}) in the Large Magellanic Cloud, LAMOST J040643.69+542347.8 has its own peculiar spectral characteristics and earlier spectral type. Moreover, LAMOST J040643.69+542347.8 is bright ($B \sim 13.9$ mag) enough to allow future high-resolution spectroscopic follow-up.

Unified Astronomy Thesaurus concepts: Massive stars (732); Stellar rotation (1629)

1. Introduction

The fast rotation of a massive star can induce the mixing that can transpose the fresh fuel H into the core, while bringing the material produced by the CNO cycle in the stellar core onto the surface, which enriches the surface abundance, prolongs the stellar life, and increases the stellar luminosity (Maeder 1987; Meynet & Maeder 2000; Brott et al. 2011; Langer 2012). Rotational mixing can produce, if strong enough, chemically homogeneous evolution (CHE). However, the strong stellar wind in a metal-rich massive star can effectively brake the rotation and therefore the mixing process (e.g., see Figure 15 in Maeder & Meynet 2012). As a result, it is hard to find a fast rotator born as a single star in high-metallicity regions.

Fortunately, most of massive stars are in binary systems (Mason et al. 2009; Chini et al. 2012). Sana et al. (2012) proposed that 71% of O-type stars would exchange materials with their companions during their whole lifetime. Binary interaction, through tides and/or by inducing mass and angular momentum accretion onto the secondary, can produce fast-rotating stars (Packet 1981; Langer 2012; de Mink et al. 2013). In fact, high-velocity components in the distributions of $v_e \sin i$ for single O- and B-type stars in 30 Dor are found by Ramírez-Agudelo et al. (2013) and Dufton et al. (2013), respectively, which are speculated to be the products of binary interactions (de Mink et al. 2013). Moreover, Li & Howarth (2020) found that most of the O stars with extreme N enrichment (i.e., ON stars) are runaways with very fast rotation speeds, which implies their origins in binary interactions.

So far, the fastest rotators are VFTS 285 and VFTS 102 with $v_e \sin i \sim 610$ km s^{-1} (Dufton et al. 2011; Walborn 2012; Ramírez-Agudelo et al. 2013), which are located in the Large Magellanic Cloud (LMC). For comparison, the previous fastest rotator in the Galaxy is HD 191423, with a projected rotation speed of only 435 km s^{-1} (Howarth & Smith 2001). In fact, it is noteworthy that all three of these stars are all runaways, which imply their binary origin.

In this Letter, the fastest rotator LAMOST J040643.69+542347.8 in the Galaxy is presented, with the projected rotational velocity $v_e \sin i \sim 540$ km s^{-1}, which is also a runaway. Further study on LAMOST J040643.69+542347.8, as well as VFTS 285 and VFTS 102, in theory and observation can help us understand the origin and nature of these extreme rotators, and also the natures of the progenitors of gravitational-wave (GW) events (de Mink et al. 2009; de Mink & Mandel 2016) and long-duration gamma-ray bursts (LGRBs; Yoon & Langer 2005; Woosley & Bloom 2006; Cano et al. 2017).

2. Data and Analysis

The star LAMOST J040643.69+542347.8 was a serendipitous discovery when we searched for Oe-type stars (Li et al. 2018) in LAMOST low-resolution spectra (LRSs; Wang et al. 1996; Su & Cui 2004; Cui et al. 2012; Luo et al. 2012; Zhao et al. 2012). Its LAMOST spectrum is shown in Figure 1. The resolving power of LRSs is about 1800, while the spectral dispersion around He II $\lambda 4542$ is about 0.583 Å/pixel.

2.1. Spectral Type

The criteria given by Sota et al. (2011) are used to assign spectral type. From Figure 1 we can see that He I $\lambda 4471$ is slightly weaker than He II $\lambda 4542$ (also see Figure 2(B)), so the star LAMOST J040643.69+542347.8 is classified as spectral type O6.5. Its unusually broad lines indicate that it is a very fast rotator, while its weak N III $\lambda\lambda 4634$–4640–4642 emissions indicate that it is also an O(f) star. Moreover, there is an absorption in He II $\lambda 4686$ emission, which is the classic characteristic of the Onfp category (Walborn 1973; Walborn et al. 2010; Sota et al. 2011), and the emission obviously weakens the absorption, so the He II $\lambda 4686$ absorption should be stronger than it looks. Walborn (2001) showed that He II $\lambda 4686$ is sensitive to surface gravity. The strong absorption of He II $\lambda 4686$ implies that the log g of some parts of this star's
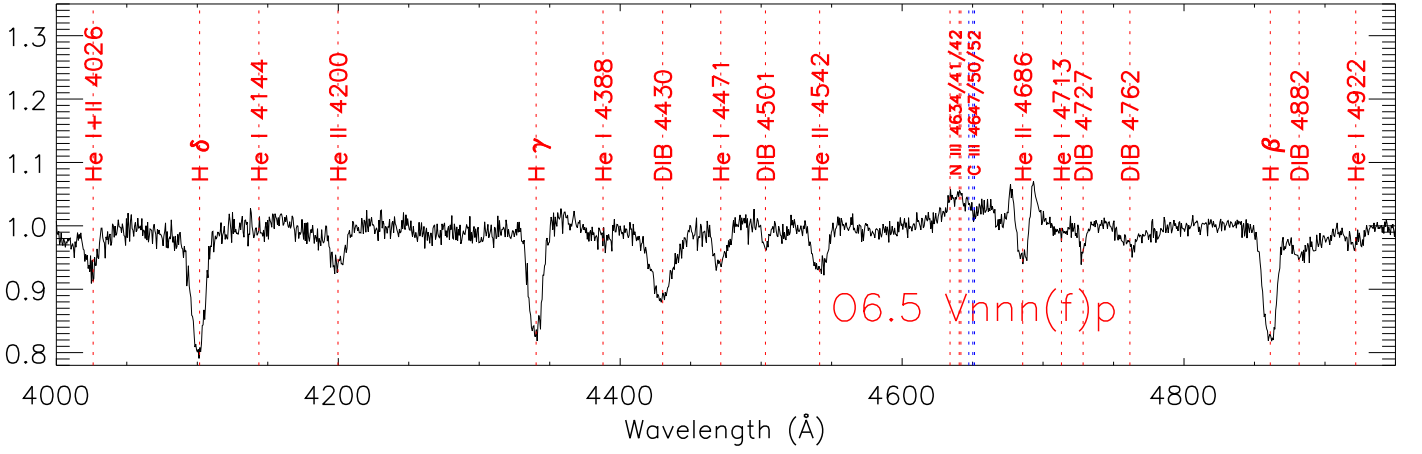
Figure 1. The LAMOST spectrum of LAMOST J040643.69+542347.8. Diffuse interstellar bands (DIBs) are also indicated.

surface is very high. Thus, it should be a dwarf. As a result, it is assigned a spectral type of O6.5 Vnnn(f)p.

2.2. Distance and Peculiar Velocity

The method given by Li & Howarth (2020) is used to deduce the distance and peculiar velocity from data of Gaia DR2 (Gaia Collaboration et al. 2018). The distances to the Sun and the Galactic center are $8901.8^{+5147.1}_{-1565.2}$ pc and $16386.9^{+5020.5}_{-1498.5}$ pc, respectively, which imply that this star is located in the Outer Arm of the Galaxy. Its peculiar velocity $(V_r, V_c, V_z) = (97.4^{+48.7}_{-16.0}, -48.6^{+15.3}_{-14.6}, 44.2^{+22.7}_{-6.9})$ km s^{-1}, and $V = \sqrt{V_r^2 + V_c^2 + V_z^2} = 118.3^{+47.3}_{-12.7}$ km s^{-1}, where, V_r, V_c, and V_z are the peculiar Galactocentric radial, circular, and vertical velocities, respectively. The velocity is greater than 28 km s^{-1}, which is the threshold for runaway stars given by Tetzlaff et al. (2011). Therefore, this star probably was originated from a binary system, then kicked off by a nonspherically symmetric explosion of its companion.

2.3. Radial Velocity, Projected Rotational Velocity, and Atmospheric Parameters

The method given by Li & Howarth (2020) is used to determine radial and projected rotational velocities (v_R and $v_e \sin i$) from He II $\lambda4542$, because this line should be formed in the deep stellar photosphere and marginally influenced by the stellar wind (De Becker & Rauw 2004). The resulting radial velocity $v_R = -91 \pm 14$ km s^{-1}.

To obtain its $v_e \sin i$, the model

$$F(\lambda, v_e \sin i) = a \times S(\lambda) \otimes P(\lambda) \otimes G(\lambda, v_e \sin i) + b \quad (1)$$

is used to fit its He II $\lambda4542$ profile. In Equation (1), $\otimes$ is the convolution operation, $S(\lambda)$ is the spectrally intrinsic profile without rotation, $P(\lambda)$ is the instrument profile, $G(\lambda, v_e \sin i)$ is the rotational-broadening profile (Gray 2005) for a given $v_e \sin i$, a is the intensity of the line, and b is the continuum.

The instrument profile $P(\lambda)$ is from the arc lamp spectrum that is used for wavelength calibration for the spectrum of this star. There are only a few emission lines in the arc lamp, so I use the linear interpolation of the profiles of two neighbor emission lines at He II $\lambda4542$ as $P(\lambda)$.

The wings of Hβ and Hγ lines in Figure 1 are very narrow and steep, which implies a low gravity, while the unusually broad lines imply it is a nearly edge-on extreme rotator. In fact,

the centrifugal force and radiative pressure can effectively reduce its total gravity near the equator (Maeder & Meynet 2000).

Liang et al. (2019) presented that the Galaxy has a radial metallicity gradient in the thin disk, and at the place where this star is located, the metallicity is similar to that of the LMC. However, the fast rotation can induce the mixing, which implies that the surficial metallicity might be enriched. Thus, the He II $\lambda4542$ profiles in the Potsdam Wolf–Rayet (PoWR) grids (Hainich et al. 2019) of LMC and solar metallicity with 31 kK $\leqslant T_{eff} \leqslant$ 42 kK and 3.4 dex $\leqslant \log g \leqslant$ 4.0 dex are used as the $P(\lambda)$s in Equation (1) to calculate $v_e \sin i$. All the resulting $v_e \sin i$ are greater than 500 km s^{-1}.

Each PoWR spectrum is convolved with the $v_e \sin i$ calculated from it and the instrument profile, then compared with the LAMOST spectrum. The best spectrum with LMC metallicity has $T_{eff} = 35$ kK and $\log g = 3.6$ dex, while the best spectrum with solar metallicity has $T_{eff} = 34$ kK and $\log g = 3.6$ dex. These two best spectra are shown in blue and red, respectively, in Figure 2(B), while $v_e \sin i$ calculated from their He II $\lambda4542$ are 543 ± 29 km s^{-1} and 538 ± 29 km s^{-1}, respectively, and their corresponding rotational profiles are also shown in blue and red in Figure 2(A). Because of gravity darkening (von Zeipel 1924), $v_e \sin i$ may be underestimated by even several tens of percents (Townsend et al. 2004).

2.4. Variablity

Another three LRSs were obtained from 2.16 m Telescope at Xinglong Observatory in China with two instruments: Beijing-Faint Object Spectrograph and Camera and the spectrograph made by Optomechanics Research Inc. for low-resolution spectroscopy (OMR). The spectra are shown in Figure 3. He II $\lambda4686$ shows obvious variability between four spectra, but the variability of radial velocity remains uncertain because of the low resolutions and signal to noise of the spectra.

Light curves for LAMOST J040643.69+542347.8 are found in the data archives of the Zwicky Transient Facility (ZTF; Masci et al. 2019) and the Wide Angle Search for Planets (WASP; Butters et al. 2010), but there are no photometric variations larger than their photometric errors.
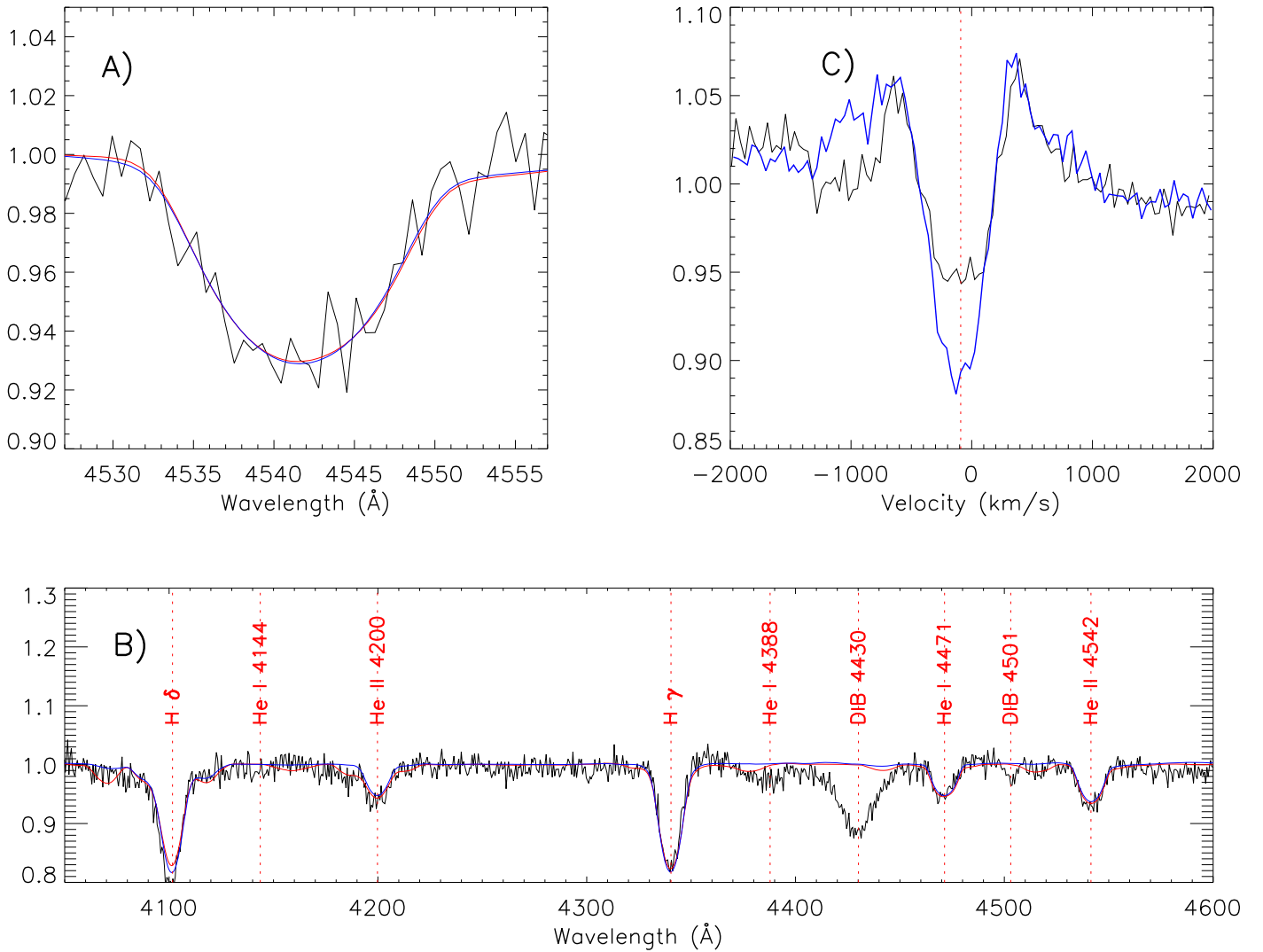
Figure 2. (A) The black line is the He II λ4542 profile in the LAMOST spectrum, while the fitted profiles calculated from two best PoWR spectra with LMC and solar metallicity are shown in blue and red, respectively. (B) The two best-fitted spectra with LMC and solar metallicity are shown in blue and red, respectively, while the LAMOST spectrum is shown in black. (C) The profiles of He II λ4686 and Hα in the LAMOST spectrum are shown in black and blue, respectively.

2.5. Luminosity

I obtained the theoretical $B - V = -0.276$ and $M_V = -5.752$ mag of LAMOST J040643.69+542347.8 from the flux-calibrated PoWR spectrum of LMC metallicity with $T_{\rm eff} = 35$ kK and $\log g = 3.6$ dex, where the B and V filter profiles are from Mann & von Braun (2015). The flux-calibrated PoWR spectrum of solar metallicity with $T_{\rm eff} = 34$ kK and $\log g = 3.6$ dex also has a similar $B - V$ and M_V as above.

In APASS DR9 (Henden et al. 2015), the $B = 13.069 \pm 0.108$ mag and $V = 13.912 \pm 0.102$ mag for LAMOST J040643.69+542347.8, respectively. Thus, if the standard extinction coefficient $R = 3.1$ is adopted, then by using the Markov Chain Monte Carlo method, its observational $M_V = -5.43^{+0.78}_{-1.05}$ mag.

3. Discussion

In Figure 2(C), He II λ4686 and Hα have similar profiles: the narrow absorptions in broad emissions, which implies that they have a similar origin. In fact, He II λ4686 and Hα are all sensitive to gravity (Walborn 2001) in O-type stars: they are in emissions in the photosphere with a low gravity, but in absorptions in the photosphere with a high one. LAMOST J040643.69+542347.8 is an extreme rotator, so its equatorial radius is larger than the polar radius, which results in higher gravities at poles while a lower one around the equator. Therefore, I speculate that their broad emissions may form from low latitude, because of low gravity and fast rotation there, and even in the stellar wind, while narrow absorptions may form near the poles because of high gravity and low rotation there.

He I λ4471 is asymmetric and blueshifted and keeps constant for more than three years, as shown in Figure 3. Gagnier et al. (2019) present that for an extreme rotator, the stellar wind around the equator is stronger than other places because of the bistability jump. Thus, I speculate that He I λ4471 may be affected by the wind originating around the equator. If it is true for LAMOST J040643.69+542347.8, then this star has much stronger losses of mass and angular momentum around the equator, which would result in a rapid spin down of the rotation in the future.

For comparison, VFTS 285 (Walborn 2012) and VFTS 102 (Dufton et al. 2011) are the two fastest rotators in the LMC,
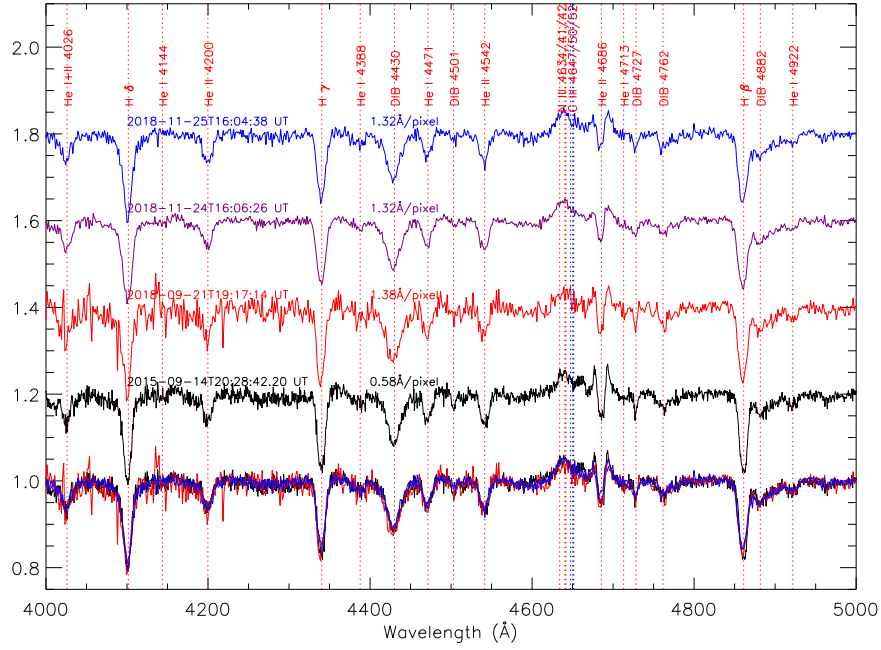
Figure 3. The upper three spectra were obtained with the 2.16 m telescope in Xinglong station, China, while the black spectrum was obtained with LAMOST. The observation time and dispersion are indicated above each spectrum. All spectra are overplotted together at the bottom by the same colors as the above.

with $v_e \sin i \sim 610$ km s^{-1} (Ramírez-Agudelo et al. 2013). Their spectral types are O7.5 Vnnn (Walborn 2012) and O9 Vnnne (Dufton et al. 2011), respectively, with normal He I $\lambda 4471$ and He II $\lambda 4686$ absorption profiles. However, the slow and dense wind around the equator is still found in VFTS 285, while the double-peaked Hα emission in the spectrum of VFTS 102 indicates that the material is being ejected from the equator and forms a circumstellar disk (Shepard et al. 2020). These phenomena show the angular momentum losses are braking down the rotations of these two stars.

Moreover, Song et al. (2016) presented that binary interaction can trigger CHE. In fact, the overenrichments of N and He and depletions of C and O on have been found on the surface of HD 191423 (Villamariz et al. 2002), which is the second fastest rotator in the Galaxy now, with $v_e \sin i \sim 435$ km s^{-1} (Howarth & Smith 2001), and also a runaway star. Therefore, it would be interesting to obtain higher-resolution spectra to determine the surface composition of this star.

4. Conclusion

In this Letter, I report the fastest rotator LAMOST J040643.69+542347.8 in the Galaxy found with LAMOST. Its properties are listed in Table 1.

LAMOST J040643.69+542347.8 is a runaway, which implies it originates from binary interaction. I cannot find the obvious variabilities of its radial velocity and photometries, which implies that it may have no (at least sufficiently massive) companion. Its blueshifted and asymmetric He I $\lambda 4471$ and absorption reversals in He II $\lambda 4686$ and Hα emissions are unique characteristics in the extreme rotator category.

LAMOST J040643.69+542347.8 is bright enough to allow future high-resolution spectroscopic follow-up, so it is a good laboratory to examine theories related to fast rotation, e.g., CHE, bistability jump of the wind around the equator, progenitors of LGRBs, and GW events.

Table 1
Observational and Theoretical Properties

Property	Estimate
R.A. (α)	61°682058
Decl. (δ)	54°396626
Gaia ϖ	0.1125 ± 0.0286 mas
Gaia μ_α	-0.816 ± 0.048 mas yr^{-1}
Gaia μ_δ	2.002 ± 0.036 mas yr^{-1}
Gaia G	12.6678 ± 0.0003 mag
Gaia BP	13.1996 ± 0.0016 mag
Gaia RP	11.9591 ± 0.0010 mag
B	13.912 ± 0.102 mag
V	13.069 ± 0.108 mag
SDSS u	14.760 ± 0.004 mag
SDSS g	14.922 ± 0.009 mag
SDSS r	12.917 ± 0.002 mag
SDSS i	12.492 ± 0.001 mag
SDSS z	12.831 ± 0.005 mag
2MASS J	11.063 ± 0.021 mag
2MASS H	10.864 ± 0.020 mag
2MASS K_s	10.720 ± 0.020 mag
Spectral Type	O6.5 Vnnn(f)p
$v_e \sin i$	540 ± 29 km s^{-1}
v_R	91 ± 14 km s^{-1}
T_{eff}	35 ± 1 kK
$\log g$	3.6 ± 0.2 dex
d	$8901.8^{+5147.1}_{-1565.2}$ pc
peculiar velocity	$118.3^{+47.3}_{-12.7}$ km s^{-1}
M_V	$-5.43^{+0.78}_{-1.05}$ mag

ORCID iDs

Guang-Wei Li (李广-伟) ⓘ https://orcid.org/0000-0001-7515-6307

References

Astropy Collaboration, Robitaille, T. P., Tollerud, J. E., et al. 2013, A&A, 558, A33
Brott, I., de Mink, S. E., Cantiello, M., et al. 2011, A&A, 530, A115
Butters, O. W., West, R. G., Anderson, D. R., et al. 2010, A&A, 520, L10
Cano, Z., Wang, S.-Q., Dai, Z.-G., et al. 2017, AdAst, 8929054, 1
Chini, R., Hoffmeister, V. H., Nasseri, A., et al. 2012, MNRAS, 424, 1925
Cui, X.-Q., Zhao, Y.-H., Chu, Y.-Q., et al. 2012, RAA, 12, 1197
De Becker, M., & Rauw, G. 2004, A&A, 427, 995
de Mink, S. E., Cantiello, M., Langer, N., et al. 2009, A&A, 497, 243
de Mink, S. E., Langer, N., Izzard, R. G., et al. 2013, ApJ, 764, 166
de Mink, S. E., & Mandel, I. 2016, MNRAS, 460, 3545
Dufton, P. L., Dunstall, P. R., Evans, C. J., et al. 2011, ApJL, 743, L22
Dufton, P. L., Langer, N., Dunstall, P. R., et al. 2013, A&A, 550, A109
Foreman-Mackey, D., Hogg, D. W., Lang, D., & Goodman, J. 2013, PASP, 125, 306
Gagnier, D., Rieutord, M., Charbonnel, C., et al. 2019, A&A, 625, A88
Gaia Collaboration, Brown, A. G. A., Vallenari, A., et al. 2018, A&A, 616, A1
Gray, D. F. 2005, The Observation and Analysis of Stellar Photospheres (3rd ed.; Cambridge: Cambridge Univ. Press)
Hainich, R., Ramachandran, V., Shenar, T., et al. 2019, A&A, 621, A85
Henden, A. A., Templeton, M., Terrell, D., et al. 2015, American Astronomical Society, AAS Meeting, 225, 336.16
Howarth, I. D., & Smith, K. C. 2001, MNRAS, 327, 353
Langer, N. 2012, ARA&A, 50, 107
Li, G.-W., & Howarth, I. D. 2020, ApJ, 888, 81
Li, G.-W., Shi, J.-R., Yanny, B., et al. 2018, ApJ, 863, 70
Liang, X., Zhao, J., Chen, Y., et al. 2019, ApJ, 887, 193
Luo, A.-L., Zhang, H.-T., Zhao, Y.-H., et al. 2012, RAA, 12, 1243
Maeder, A. 1987, A&A, 178, 159
Maeder, A., & Meynet, G. 2000, ARA&A, 38, 143
Maeder, A., & Meynet, G. 2012, RvMP, 84, 25
Mann, A. W., & von Braun, K. 2015, PASP, 127, 102
Masci, F. J., Laher, R. R., Rusholme, B., et al. 2019, PASP, 131, 018003
Mason, B. D., Hartkopf, W. I., Gies, D. R., et al. 2009, AJ, 137, 3358
Meynet, G., & Maeder, A. 2000, A&A, 361, 101
Packet, W. 1981, A&A, 102, 17
Ramírez-Agudelo, O. H., Simón-Díaz, S., Sana, H., et al. 2013, A&A, 560, A29
Sana, H., de Mink, S. E., de Koter, A., et al. 2012, Sci, 337, 444
Shepard, K., Gies, D. R., Lester, K. V., et al. 2020, ApJ, 888, 82
Song, H. F., Meynet, G., Maeder, A., et al. 2016, A&A, 585, A120
Sota, A., Maíz Apellániz, J., Walborn, N. R., et al. 2011, ApJS, 193, 24
Su, D.-Q., & Cui, X.-Q. 2004, ChJAA, 4, 1
Tetzlaff, N., Neuhäuser, R., & Hohle, M. M. 2011, MNRAS, 410, 190
Townsend, R. H. D., Owocki, S. P., & Howarth, I. D. 2004, MNRAS, 350, 189
Villamariz, M. R., Herrero, A., Becker, S. R., et al. 2002, A&A, 388, 940
von Zeipel, H. 1924, MNRAS, 84, 665
Walborn, N. 2001, in ASP Conf. Ser. 242, Eta Carinae and Other Mysterious Stars: The Hidden Opportunities of Emission Spectroscopy, ed. T. R. Gull, S. Johannson, & K. Davidson (San Francisco, CA: ASP), 217
Walborn, N. 2012, in ASP Conf. Ser. 465, Proc. Scientific Meeting in Honor of Anthony F. J. Moffat, ed. L. Drissen, C. Robert, & N. St-Louis (San Francisco, CA: ASP), 460
Walborn, N. R. 1973, AJ, 78, 1067
Walborn, N. R., Howarth, I. D., Evans, C. J., et al. 2010, AJ, 139, 1283
Wang, S.-G., Su, D.-Q., Chu, Y.-Q., Cui, X., & Wang, Y.-N. 1996, ApOpt, 35, 5155
Woosley, S. E., & Bloom, J. S. 2006, ARA&A, 44, 507
Yoon, S.-C., & Langer, N. 2005, A&A, 443, 643
Zhao, G., Zhao, Y.-H., Chu, Y.-Q., Jing, Y.-P., & Deng, L.-C. 2012, RAA, 12, 723